Interface dynamics in a mean-field lattice gas model: Solute trapping, kinetic coefficient, and interface mobility

Mathis Plapp* and Jean-François Gouyet†
Laboratoire de Physique de la Matière Condensée, Ecole Polytechnique, 91128 Palaiseau, France
(Received 16 September 1996)

In a recent paper we showed that we can obtain dendritic growth in a mean-field lattice gas model. The equation of motion, derived from a local master equation, is a generalized Cahn-Hilliard equation. In the present paper, we study the isothermal dynamics of planar interfaces in this model. Stationary interface states advancing with constant velocity are investigated. We present numerical results as well as a continuum approximation that gives an analytic expression for the shape correction in the limit of small interface velocities. We observe departure from local equilibrium at the interface and solute trapping. The associated kinetic coefficients are calculated. The two effects are found to be related. We finally give an expression for the interface mobility and derive a relation between this mobility and the kinetic coefficients. Furthermore, we show that there occur oscillations of the growth velocity and density waves in the two bulk phases during the advance of the interface. This is related to the discrete dynamics using the theory of area-preserving maps as proposed by Pandit and Wortis. [S1063-651X(97)11305-8]

PACS number(s): 05.70.Ln, 68.35.Fx, 05.50.+q, 82.65.Dp

I. INTRODUCTION

The study of moving interfaces is an old subject. The field in which most of the interesting questions first arose is metallurgy, where the microstructure of materials is greatly influenced by the domain growth processes during their fabrication. Two well-known and extensively studied processes where interface dynamics is crucial are spinodal decomposition (phase separation) and dendritic growth. The classic models are phenomenological continuum models: the Cahn-Hilliard equation [1] for phase separation, and diffusion equations assorted with a Gibbs-Thomson boundary condition at the interface for dendritic growth [2–5]. In the latter approach, the interface is modeled by a sharp surface (a line in two dimensions), and we have to specify the boundary conditions at this surface as functions of its curvature and velocity.

The motion of two-phase interfaces can be controlled by diffusion or by growth kinetics. In the first case, the interface is in local thermodynamic equilibrium, and growth is entirely limited by diffusion: heat or material has to diffuse through the bulk phases to allow the phase transformation to proceed. The limiting step in the second case is the flow of material across the interface: if the time necessary for a particle to be incorporated in the growing phase is much larger than the characteristic diffusion time scale, temperature and solute concentration are nearly constant in the bulk phases, and the interface velocity is determined by the incorporation kinetics. The reality is situated almost always somewhere between these two extremes. Often, the kinetic effects are small. This leads to a small modification of the local equilibrium at the advancing interface. For example, in dendritic growth, it has been recognized that to account for the obtained growth shapes, one often has to generalize the local equilibrium condition at the interface (Gibbs-Thomson condition) by inclusion of a velocity-dependent term [6].

Another phenomenon related to the finite kinetic time scale is the so-called ''solute trapping'' effect, observed during rapid solidification in alloys [7–11]: the solute atoms cannot escape fast enough from the advancing front and are incorporated into the growing solid even if this increases their chemical potential. This leads to a concentration of the growing solid that is different from the equilibrium one. In this case, the departure from local equilibrium may be important, and the linear approximation that is currently used in dendritic growth is limited to small growth velocities.

There have been numerous attempts to describe interfacial dynamics in continuum theories. The problem of a purely diffusion-controlled interface is known as the Stefan problem, and there is a huge body of literature [12]. Langer and Sekerka used the Cahn-Hilliard equation to calculate the deviations from the equilibrium interface shape [13]. Their method needs as input the atomic mobility as a function of the concentration. More recent approaches include phase-field methods that use a (mesoscopic) local thermodynamic description and couple a local-order parameter to a diffusion field [11,14–17]. It would be interesting to establish the connection between such macroscopic methods and microscopic dynamical models. In statistical mechanics, a great deal of attention has been paid to the dynamics of model systems as the kinetic Ising model [18,19]. However, in their original version these models are (for the moment) still too difficult because of their probabilistic nature, and exact solutions are known only for some special cases.

We want to present here a microscopic model that displays some of the features described above. It is based on a mean-field method recently developed by one of the authors [20]. From a master equation of a stochastic lattice gas, one can derive a system of coupled nonlinear differential equations, which takes the form of a generalized Cahn-Hilliard equation. This procedure gives an explicit expression for the

*Electronic address: Mathis.Plapp@Polytechnique.fr
†Electronic address: Jean-Francois.Gouyet@Polytechnique.fr

atomic mobility, in contrast to the standard Cahn-Hilliard equation, where the mobility is usually taken constant. Our equations are discrete, but they are not merely a discretization of the continuous Cahn-Hilliard equation: the underlying lattice gas model establishes a connection to real crystal lattices, say, in an alloy. This motivates the choice of the transition rates. We choose activated jump processes, leading to an Arrhenius behavior as generally observed in metallic compounds. Thus our model could be a highly simplified description of a binary alloy. However, its present version is isothermal, so it can only describe processes in alloys where the chemical diffusion is the rate-limiting step and thermal diffusion is fast enough to assure thermal equilibrium. We have shown in a recent paper [21] that this model exhibits dendritic growth, and calculated the orientation-dependent surface tension. Here, we will analyze more in detail the dynamics of planar interfaces.

We investigate stationary interfaces, moving with constant velocity, driven by a constant interdiffusion current fed into the system. This models interface motion during late-stage growth, when the local interface velocity varies very slowly, and the incoming currents are determined by the solution of the long-range diffusion problem. Numerical simulations show that the shape of the interface is modified by the motion. Our model displays the kinetic shift of local equilibrium and an effect that is analogous to solute trapping during solidification. Using a continuum approximation, we can calculate the correction to the equilibrium interface profile to linear order in the interface velocity. This shows a very good agreement with the simulations. The solute trapping effect is governed by the kinetics of particles traversing the interface, as it should. We have access to various interesting quantities. For example, we can show that a chemical potential drop develops at the interface, which corresponds to energy dissipation at the interface during incorporation of new material. For small velocity, the height of this potential step is proportional to the velocity, and the proportionality constant defines an interface mobility, which we can calculate. We also have access to the kinetic coefficient needed in the Gibbs-Thomson condition.

Coming back to the original, discrete model we then investigate whether the continuum approximation is a good description. The discreteness of the equations causes variations of the chemical potential at the interface during its advance, which can be understood using the theory of area-preserving maps developed by Pandit and Wortis [22]. This leads also to variations of the surface energy. The main effects are growth velocity oscillations with the periodicity of the lattice, and damped density waves behind the interface, whose wavelength can be considerably larger than the lattice spacing. However, the amplitude of these oscillations is very small, and they do not modify substantially the values for the kinetic coefficients obtained in the continuum approximation, which therefore is a valid approach. Variations in physical quantities during interface motion due to lattice effects are known to occur in epitaxial growth [23,24], and density oscillations have been reported in some discrete growth models [25–27]. However, in our case the connection to local thermodynamics is particularly straightforward.

In Sec. II, we will describe the model. After a short presentation of our simulations in Sec. III, we discuss in Sec. IV the continuum approximation and use it to calculate the first-order shape correction to the equilibrium interface shape. In Sec. V, we investigate in more detail the discrete system and the growth velocity oscillations. Section VI contains the results for the kinetic coefficients describing the interface motion, together with comparisons to simulations. Section VII is devoted to a summary and discussion.

II. THE MODEL

This model has been presented in some detail in [21], and we will give here only a very brief summary. As we want to apply our results to the complete two-dimensional model, we will study planar interfaces on a square lattice. Evidently, for a planar interface, a one-dimensional description is sufficient; however, as we shall see, there are slight differences between dynamics in different directions, and therefore it is useful to keep in mind that there is an underlying two-dimensional lattice.

Consider a square lattice of N sites in two dimensions (coordination number $z=4$). Let n_i denote the occupation number of site i: $n_i=1$ if a particle is present, 0 otherwise. With an attractive nearest-neighbor interaction, the Hamiltonian is

$$H=-\varepsilon\sum_{\langle i,j\rangle} n_i n_j-\mu_0\sum_{i=1}^{N} n_i, \tag{1}$$

where ε is the interaction energy (attractive: $\varepsilon>0$), μ_0 is an external chemical potential, and the first sum goes over all nearest-neighbor pairs. Clearly, this is completely equivalent to the Ising model. Besides, this is only another form of the Hamiltonian of a binary alloy, if we think of a particle (hole) as an atom of type A (B).

To define the dynamics, we assume that particles can move only by nearest-neighbor hops. In the alloy picture, this corresponds to a simple exchange mechanism. The system is in contact with a heat bath: temperature is constant, and energy is not conserved. Particles can be introduced or taken out only at the boundaries. The transition rate for a particle jumping from site i to site k is given by

$$w_{ik}(\{n\})=w_0\exp\left(\frac{\varepsilon}{kT}\sum_{\mathbf{a}} n_{1+\mathbf{a}}\right). \tag{2}$$

w_0 is the bare jump frequency (or the jump rate of an A atom in a B environment in the alloy picture), and sets the overall time scale. Here and in the following, **a** will denote a lattice unit vector, and summation over **a** means summation over all nearest neighbors. This choice of transition rates corresponds to an activated process and displays the Arrhenius behavior that is common in metallic diffusion. The lattice points are located at the equilibrium positions of atoms in a crystal structure. Then an atom is trapped at its site in a potential well whose depth depends on the local energy landscape. We assume that the saddle points between the wells are at a constant energy; then the depth of a potential well is equal to the energy necessary to take away an atom from its site, that is, the sum of its binding energies.

Expression (2) differs from the usual Metropolis rule, where the transition rate is proportional to $\exp(-\Delta H/2kT)$

with ΔH being the energy difference between initial and final state. This corresponds to a process without activation barrier. In our model, the transition rate depends only on the initial state. Since our transition rates satisfy detailed balance, the equilibrium distribution is the same. But contrary to the widely used Kawasaki exchange dynamics [28], where the dynamics is invariant under a global spin-flip, we have an asymmetry between particles and holes: an atom surrounded by attractive neighbors will stay in its place much longer than a hole surrounded by other holes.

Writing a local master equation, and making a mean-field approximation (see [20,21] for more details), we arrive at the following equation of motion:

$$\frac{\partial p_i}{\partial t} = -w_0 \sum_k \left\{ p_i(1-p_k)\exp\left(-\kappa \sum_{\mathbf{a}} p_{i+\mathbf{a}} \right) - p_k(1-p_i)\exp\left(-\kappa \sum_{\mathbf{a}} p_{k+\mathbf{a}} \right) \right\}. \tag{3}$$

Here, the occupation probabilities p_i (which can be interpreted as concentrations as well) are continuous variables between 0 and 1, and $\kappa = \varepsilon/kT$. The terms on the right-hand side are currents resulting from jumps of particles from site i to a neighboring site (first terms) or the inverse (second terms). Indeed, it is a conservation equation for the particle concentration,

$$\frac{\partial}{\partial t} p_i = -\sum_k j_{ik}, \tag{4}$$

where j_{ik} denotes the particle current in the link ik. The currents can be rewritten in the form of generalized transport equations,

$$j_{ik} = -M_{ik}(\mu_k - \mu_i), \tag{5a}$$

$$j_{ik} = -D_{ik}(p_k - p_i), \tag{5b}$$

with a generalized mobility

$$M_{ik} = w_0(1-p_k)(1-p_i)e^{-z\varepsilon/2kT} \frac{e^{\mu_k/kT} - e^{\mu_i/kT}}{\mu_k - \mu_i} \tag{6}$$

and a generalized diffusion coefficient

$$D_{ik} = w_0(1-p_k)(1-p_i)e^{-z\varepsilon/2kT} \frac{e^{\mu_k/kT} - e^{\mu_i/kT}}{p_k - p_i}. \tag{7}$$

Here, we have defined the local chemical potential as

$$\mu_k = -\varepsilon \sum_{\mathbf{a}} (p_{k+\mathbf{a}} - p_k) - z\varepsilon(p_k - \tfrac{1}{2}) + kT \ln \frac{p_k}{1-p_k} \tag{8}$$

(z is the coordination number of the lattice). In the first term we recognize a discrete Laplacian: this chemical potential takes into account local curvature of the concentration profile, a natural extension as already noticed by Cahn [29]. We have fixed in Eq. (8) the constant μ_0 in the Hamiltonian (1) (which is arbitrary for a fixed number of particles) to $\mu_0 = z\varepsilon/2$ in order to make the chemical potential antisymmetric with respect to the interchange of particles and holes. This gives rise to the factors $\exp(-z\varepsilon/2kT)$ in Eqs. (6) and (7).

The mobility and diffusion coefficient both include dependence on concentration as well as gradient and curvature terms. The connection with the well-known field-theoretic models [30] can be established by setting

$$\mu_k = \frac{\partial F(\{p\})}{\partial p_k}, \tag{9}$$

$F(\{p\})$ being a lattice version of a free-energy functional:

$$F(\{p\}) = \sum_k \left(f(p_k) + \frac{\varepsilon}{4} \sum_{\mathbf{a}} (p_{k+\mathbf{a}} - p_k)^2 \right) \tag{10}$$

with a local potential

$$f(p) = -\frac{z\varepsilon}{2}(p - \tfrac{1}{2})^2 + kT[p \ln p + (1-p)\ln(1-p)]. \tag{11}$$

This is a discrete analog of a continuous functional of the Ginzburg-Landau type, with ε playing the role of a gradient energy:

$$F = \int \left(f(p) + \frac{\varepsilon a^2}{2} (\nabla p)^2 \right) dV. \tag{12}$$

Using these identities and the expressions (5), the equation of motion can be rewritten as a generalized Cahn-Hilliard equation, or alternatively as a nonlinear diffusion equation. The structure of the free-energy function can be obtained simply by discretizing a continuous functional; however, the expressions for mobility and diffusion coefficients are intimately connected to the underlying jump process. Remember that Eq. (3) describes indeed a system moving towards equilibrium: calculating the total time derivative of the free energy, we find

$$\frac{dF}{dt} = -\frac{1}{2} \sum_{i,k} M_{ik}(\mu_k - \mu_i)^2. \tag{13}$$

Since M_{ik} is always positive, the free energy can only decrease, and the stationary states satisfy $\mu_k \equiv \mu = \text{const}$.

Below the critical temperature $kT_c = z\varepsilon/4$, the potential f has a double-well structure with two minima, symmetric with respect to $\frac{1}{2}$, p_{eq}^{α} and p_{eq}^{β}. Here and in the following, α will denote the dense (''A-rich''), β the dilute (''B-rich'') phase. Near T_c, the potential can be closely approximated by a quartic polynomial. For lower temperatures, higher-order terms become more important. The two potential wells become very sharp and are located very close to 0 and 1. The phase diagram is depicted in Fig. 1. The order parameter is the miscibility gap $\Delta p(T) = p_{\text{eq}}^{\alpha}(T) - p_{\text{eq}}^{\beta}(T)$. The transition is first order except at the point $p = \frac{1}{2}$, which corresponds to zero magnetic field in the Ising model.

This is exactly equivalent to the mean-field phase diagram of the Ising model. So, statics are completely symmetric with respect to the interchange of particles and holes. But dynamics are not. If in the expressions (6) and (7) for mobility and

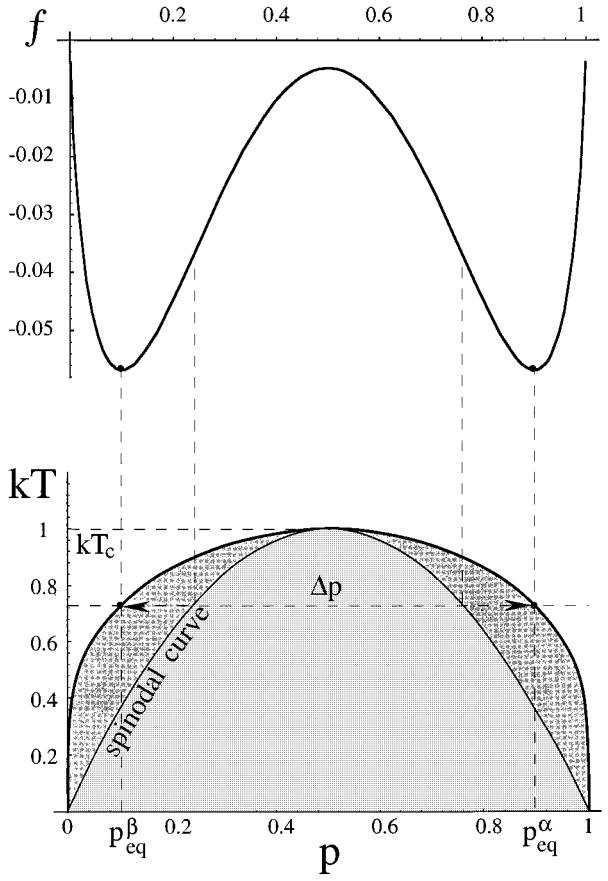

FIG. 1. Local free energy f as a function of p for a temperature $T<T_c$ and the mean-field phase diagram of a simple binary mixture: the two equilibrium concentrations p_{eq}^{α} and p_{eq}^{β} are located at the minima of f. The regions in light gray are unstable; dark gray corresponds to metastable states.

diffusion coefficient we take the limit of homogeneous systems ($p_i \to p$ for all i) and use expression (8), we find

$$M_{\mathrm{hom}}(p) = w_0 \frac{p(1-p)}{kT} \exp(-\kappa z p) \tag{14}$$

for the mobility and, using the chain rule,

$$D_{\mathrm{hom}}(p) = w_0[1-\kappa z p(1-p)]\exp(-\kappa z p) \tag{15}$$

for the diffusion coefficient. Notice that these quantities are still defined on the bonds of the lattice. To give them the usual dimensions of the continuum equivalents, that is, length squared over time, one has to multiply them by the square of the jump length, a^2. Taking advantage of the symmetry of the two equilibrium concentrations, we have

$$\frac{D_{\mathrm{hom}}(p_{\mathrm{eq}}^{\alpha})}{D_{\mathrm{hom}}(p_{\mathrm{eq}}^{\beta})} = \exp(-\kappa z \Delta p), \tag{16}$$

where the miscibility gap Δp is a function of temperature. We see that near the critical temperature this ratio approaches unity, whereas for low temperatures, the diffusion in the dense phase is very much slower than in the dilute phase, which is the situation found in solidification.

For planar interfaces, the system of equations (3) can be simplified. When the interface is oriented normal to the (10)- or (11)-symmetry directions, we can reduce it to a quasi-one-dimensional set of equations for points on a line. Then each concentration p_k represents a whole layer of lattice sites and the indices are integers, proportional to the normal coordinate. For the (10) direction the reduced version of Eq. (3) reads

$$\frac{dp_k}{dt} = w_0 \sum_j \{p_k(1-p_j)\exp[\kappa(p_{k-1}+2p_k+p_{k+1})] - p_j(1-p_k)\exp[\kappa(p_{j-1}+2p_j+p_{j+1})]\}, \tag{17a}$$

whereas for the (11) direction it is

$$\frac{dp_k}{dt} = w_0 \sum_j \{2p_k(1-p_j)\exp[2\kappa(p_{k-1}+p_{k+1})] - 2p_j(1-p_k)\exp[2\kappa(p_{j-1}+p_{j+1})]\}. \tag{17b}$$

In the second case, there are two bonds connecting a site to the neighboring layer. In both cases, j takes the values $k-1$ and $k+1$ in the sum. The distance between two successive layers is a in the (10) direction and $a/\sqrt{2}$ in the (11) direction.

III. SIMULATIONS

To investigate Eqs. (17), we integrated them numerically for various temperatures, initial conditions, and system sizes L. We used a simple Euler algorithm with variable time step to allow for initial conditions far from equilibrium. The calculation speed is limited by a numerical instability occurring in the low-density phase, where diffusion is fastest. The limit on the time step can be calculated by linear stability analysis. We used a maximal time step near this threshold. Control runs with smaller time step gave the same results.

We initialized the system with an interface, the α phase being to the left. The system was closed at this side: at $k=0$, we imposed a zero flux boundary condition. To calculate the current from site 0 to site 1, we need the value of p at location -1. We chose ''mirror'' boundary conditions, that is $p_{-1}=p_0$. So we can imagine the system to be one half of a one-dimensional droplet (or a two-dimensional slice) growing symmetrically. At $x=L$, we fixed the current to some value j_0. To obtain a stationary state, we performed simulations in a moving frame: once the interface reached a fixed position, the whole configuration was set back by one lattice step. Under these conditions, we observed that the system converged to a stationary state, independent on the initial condition (as long as there is an interface at the beginning). The interface profile and velocity depend only on temperature and the injected current.

A typical stationary interface state is depicted in Fig. 2. In nonconserved systems the two-phase front may propagate by simple displacement, and to first order in the velocity the form of the moving front is the same as at equilibrium. In systems with global mass conservation, this growth mode is forbidden. New material has to be brought to the interface by diffusive transport. We can roughly distinguish three different regions (Fig. 2): behind the moving front (region I), a

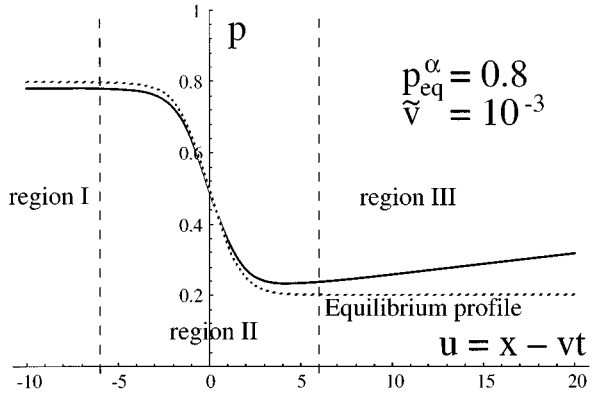

FIG. 2. Stationary interface shape for $T=0.86T_c$ and dimensionless velocity $\tilde{v}=v/aw_0=10^{-3}$, obtained from the continuum treatment described in Sec. IV (u is in units of a). The equilibrium profile is also shown (broken line).

plateau at concentration p_∞^α develops. p_∞^α is a function of the velocity and always smaller than the equilibrium concentration of the dense phase, $p_{\rm eq}^\alpha$. This is an effect analogous to solute trapping in solidification. Here, we have not strictly a liquid-solid transition, because entropy and internal energy are the same in the two phases (no latent heat associated with the transition). However, the process is exactly analogous to solidification: the growing α phase ''traps'' holes that cannot escape fast enough through the advancing interface. This is a purely dynamic effect. The chemical potential of the trapped species (here, holes or B atoms) is increased. The growing phase is not at its equilibrium concentration and hence not stable. If the external driving force was turned off, the system would relax to the equilibrium state by (slow) diffusion of holes through the α phase. For small velocities and temperatures close to T_c, the resulting concentration p_∞^α is a linear function of the velocity. At low temperatures and high velocities, $p_\infty^\alpha(v)$ becomes highly nonlinear due to the slow dynamics in the α phase.

Region II is the interface itself, which conserves a structure close to the equilibrium state when the velocity is small. Ahead of the moving interface (region III), we find a ''ramp'' profile that can be approximated by a straight line sufficiently far from the interface. However, this is true only for small system sizes. The stationary solution of the diffusion equation in a frame moving with velocity v is an exponential with decay length $l_D=D/v$; this looks like a straight line on a length scale much smaller than l_D. In our simulations, typical values are (in terms of the lattice constant a and the bare jump rate w_0) $D\approx 1$ and $v\approx 10^{-5}$, giving a diffusion length of the order 10^5. The approximation of the ramp profile by a straight line is therefore valid for system sizes L which satisfy $\xi \ll L \ll l_D$, where ξ is the characteristic interface thickness. For our simulations, we used $L=80$ in the (10) direction and $L=100$ in the (11) direction.

To compare our findings with the phenomenological sharp-interface models, we have to extract the boundary conditions of the latter from extrapolation of the concentration profiles in the bulk phases to a hypothetical sharp dividing surface, which has to be conveniently defined (see the discussion at the end of Sec. V). The intercept of the ramp profile at this sharp interface position, $p_{\rm int}^\beta$, is a function of the interface velocity. The linear term of this function gives the kinetic coefficient β_0, currently used in the dynamical extension of the Gibbs-Thomson boundary condition.

The interface velocity we obtain for a fixed current depends on the system size, or more precisely on the distance between the interface and the point where the current is injected. On the other hand, when we compare interface profiles at equal velocity for different system sizes, they are identical. This is a consequence of mass conservation: for a continuous stationary state, the quantity $j-vp/a$ is constant throughout the interface; this is still approximately true for our discrete model. In region III, p depends on the distance from the interface, and if we fix the same current at two different points, we will obtain different velocities.

Therefore, we choose as variable for all our subsequent developments the dimensionless interface velocity, $\tilde{v}=v/(aw_0)$, which determines the shape of the stationary state, independent on system size. We are limited to small velocities by the phase diagram of our model: the concentration in region III may not be greater than the stability limit given by the spinodal curve (see Fig. 1). In other words, the supersaturation of the β phase is restricted to small values. The dimensionless velocities we could obtain in our simulations vary between 10^{-5} and 10^{-3}, in function of temperature. For very low temperatures and close to T_c, only very small velocities are possible. Notice, however, that ''small'' is stated in terms of aw_0. Since w_0 may take values between 10^8 and 10^{13} Hz, depending on the host lattice and temperature, considerable macroscopic velocities may be attained. Interesting quantities to determine are the concentration value far behind the interface p_∞^α, and the intercept $p_{\rm int}^\beta$ as functions of $\tilde{v}$. These data are the principal test for our analytical developments. The numerical results will be discussed in Sec. VI in direct comparison with our analytic expressions.

IV. CONTINUUM APPROXIMATION

A. Equilibrium state

The equilibrium states are given by $\mu=$const. As we shall see in Sec. V, the mathematics of discrete systems is much more intricate than for the continuum. As a first step, we therefore will analyze the continuum approximation. One verifies easily that in the continuum limit the two equations (17a) and (17b) become the same, as expected: we lose the effect of lattice anisotropy. We will immediately specialize to the case of a planar interface, and we will denote by x the normal coordinate. Then, the chemical potential can be chosen equal to 0 by symmetry. We replace the discrete derivatives (finite differences) by $a\times\partial/\partial x$, where a is the lattice constant. Then Eq. (8) for the chemical potential becomes

$$-\varepsilon a^2\,\frac{\partial^2 p(x)}{\partial x^2}+f'(p(x))\equiv 0. \tag{18}$$

f' denotes the derivative of $f(p)$ [Eq. (11)] with respect to p and is the local part of the chemical potential. To discuss the validity of this procedure, we remark that a characteristic length scale of the interface solution to this equation can be

obtained by linearizing it around one of its stable fixed points $p_{\rm eq}^{\alpha}$ or $p_{\rm eq}^{\beta}$. The asymptotics are exponentials with a decay length

$$\xi_0 = a\sqrt{\varepsilon \chi_{\rm eq}}, \tag{19}$$

where the susceptibility $\chi(p)$ is defined as

$$\chi(p) = \frac{1}{f''(p)} = \frac{p(1-p)}{kT - z\varepsilon p(1-p)}, \tag{20}$$

and $\chi_{\rm eq} = \chi(p_{\rm eq})$. If ξ_0 is much larger than a, the committed error due to the continuum approximation should be small. For T tending to the critical temperature, ξ_0 diverges with power $\frac{1}{2}$, as expected for a mean-field correlation length. We thus can expect that Eq. (18) is a good description near the critical temperature.

It is known that for a quartic potential $f(p)$, Eq. (18) is solved by the hyperbolic tangent. In our case, f contains terms of all orders. If we truncate at the fourth-order term, we get a good description of the central interface region, but we do not recover the right limit values (the bulk equilibrium concentrations) at infinity. On the other hand, a pure hyperbolic tangent profile connecting the bulk equilibrium concentrations is not correct in the interfacial region. We can, however, approximate the exact solution to any desired precision by an expansion in powers of the hyperbolic tangent. We pose

$$p_0(x) = \frac{1}{2} - \left[c_1 \tanh\left(\frac{x}{2\xi_0}\right) + c_3 \tanh^3\left(\frac{x}{2\xi_0}\right) + c_5 \tanh^5\left(\frac{x}{2\xi_0}\right) + \cdots \right], \tag{21}$$

where ξ_0 is defined by Eq. (19): this assures the correct exponential decay. If we expand the potential $f(p)$ given by Eq. (11) up to order $2n$ in p and equate the tanh terms order by order (up to order $2n-1$), we get $n-1$ equations among the coefficients, which allows us to express all in function of, say, c_1. Then we use the boundary condition, $p_0(-\infty) - p_0(+\infty) = \Delta p$, to obtain

$$\sum_{m=1}^{n} c_{2m-1} = \Delta p/2. \tag{22}$$

This gives a polynomial equation for c_1, which we solve numerically. As expected, for high temperatures all coefficients besides the first are very small. We will use in the following only the lowest-order approximation,

$$p_0(x) = \frac{1}{2} - \frac{\Delta p}{2} \tanh\left(\frac{x}{2\xi_0}\right), \tag{23}$$

representing an interface between the α phase at $-\infty$ and the β phase at $+\infty$.

B. Stationary states

We now want to calculate the shape of an interface advancing at constant velocity. An exact solution of the full nonlinear equations is out of reach; we therefore will linearize the problem around the equilibrium solution. Furthermore, in the continuum limit we can somewhat simplify the equations. Let us for a moment return to the discrete formulation and examine more closely the mobility (6).

If $\mu = 0$ in all the system (equilibrium state), Eq. (6) simplifies to

$$M_{ik} = w_0 \frac{(1-p_k)(1-p_i)}{kT} e^{-z\varepsilon/2kT}, \tag{24}$$

which can be rewritten as

$$M_{ik} = w_0 e^{-z\varepsilon/2kT} \frac{(1-p_i)^2}{kT} \left(1 - \frac{p_k - p_i}{1-p_i}\right). \tag{25}$$

Near equilibrium, the chemical potential is only slightly different from 0; analyzing the expression of the current (5a), we see that to first order in a the above expression for the mobility is sufficient. If we inject this in the conservation equation (4), we find to first order

$$\frac{\partial p_i}{\partial t} = w_0 e^{-z\varepsilon/2kT} \frac{(1-p_i)^2}{kT} \left[\sum_a (\mu_{i+a} - \mu_i) - \frac{1}{1-p_i} \sum_a (\mu_{i+a} - \mu_i)(p_{i+a} - p_i) \right], \tag{26}$$

where sum over a means summation over all links adjacent to i. If we now again use the continuum approximation (momentarily, we come back here to the full two-dimensional treatment), this can be rewritten in a simpler form:

$$\frac{\partial p(\vec{x},t)}{\partial t} = w_0 e^{-z\varepsilon/2kT} \frac{[1-p(\vec{x},t)]^2}{kT} \times \left[a^2 \Delta\mu - \frac{2a^2}{1-p(\vec{x},t)} \mathbf{grad}\,\mu \cdot \mathbf{grad}\, p \right], \tag{27}$$

where Δ is the Laplacian operator. Another rearrangement gives

$$\frac{\partial p(\vec{x},t)}{\partial t} = a^2 \mathrm{div}[M_{\rm loc}(p(\vec{x},t)) \mathbf{grad} \mu], \tag{28}$$

which has exactly the structure of a Cahn-Hilliard equation with a *local* mobility

$$M_{\rm loc}(p) = w_0 \frac{e^{-z\varepsilon/2kT}}{kT} (1-p)^2 \tag{29}$$

depending only on the local concentration. This result is simply the continuum limit of Eq. (6) for $\mu = 0$. On the contrary, if we consider homogeneous states, for which the Laplacian is 0, we find the homogeneous mobility (14). As could have been expected, near equilibrium the curvature effects in the mobility can be neglected, leading to a local mobility function instead of the complete expression (6) that has to be used far from equilibrium. In addition, this mobility function is a simple polynomial in p [the exponential term of Eq. (14) is absent], which simplifies our analytic treatments.

For a planar interface with normal coordinate x, the equation of motion takes the form

$$\frac{\partial p(x,t)}{\partial t} = a^2 \frac{d}{dx}\left(M_{\rm loc}(p(x,t)) \frac{d\mu(x,t)}{dx} \right). \tag{30}$$

We search stationary states, that is, solutions of this equation that propagate with constant velocity v. Such solutions depend on x and t only through the combination $u = x - vt$. The equation transformed in this moving frame reads

$$-v \frac{dp(u)}{du} = a^2 \frac{d}{du}\left(M_{\rm loc}(p(u)) \frac{d\mu(u)}{du} \right). \tag{31}$$

This equation can be integrated once to furnish the relation

$$j(u) = \frac{v}{a}\left[p(u) - p_\infty^\alpha \right] \tag{32}$$

(remember that $j = -Ma d\mu/dx$). This is nothing else than the expression for mass conservation in the moving frame: the left-hand side is the interdiffusion current, the right-hand side represents the current crossing the interface because of its advance. Integrating this equation once more, we obtain

$$\mu(u) = \mu(-\infty) - \frac{v}{a} \int_{-\infty}^{u} \frac{p(u') - p_\infty^\alpha}{M_{\rm loc}(p(u'))} \frac{du'}{a}. \tag{33}$$

Using the continuum expression (18) for μ, we obtain an integro-differential equation for $p(u)$:

$$-\varepsilon a^2 p''(u) - \frac{\partial f}{\partial p}(p(u)) + \frac{\partial f}{\partial p}(p_\infty^\alpha) + \frac{v}{a} \int_{-\infty}^{u} \frac{p(u') - p_\infty^\alpha}{M_{\rm loc}(p(u'))} \frac{du'}{a} = 0. \tag{34}$$

Equivalent expressions have already been obtained by Langer and Sekerka [13]. We emphasize once more that this expression will be valid only not too far from equilibrium since we use the ''local'' expression (29) for the mobility.

We are interested in the shape correction to the equilibrium interface for small velocities and with the boundary condition $j(-\infty) = 0$ (no current in the α phase). We will assume that this correction is linear in the velocity and make the ansatz

$$p(u) = p_0(u) + \tilde{v} p_1(u), \tag{35}$$

where $p_0(u)$ is the equilibrium solution, and $\tilde{v} = v/(a w_0)$ is the dimensionless interface velocity. Far behind the interface the concentration is constant, deviating from the equilibrium concentration by an amount proportional to the velocity. This means that $p_1(u)$ tends to a constant value p_1^α for $u \to -\infty$. The linearized equation for the first order in $\tilde{v}$ becomes

$$\varepsilon a^2 p_1''(u) + \frac{p_1(u)}{\chi(p_0(u))} - \frac{p_1^\alpha}{\chi_{\rm eq}} + \nu(u) = 0, \tag{36}$$

where χ is given by Eq. (20) and we have defined $\nu(u)$ by

$$\nu(u) = \int_{-\infty}^{u} \frac{w_0 [p_{\rm eq}^\alpha - p_0(u')]}{M_{\rm loc}(p_0(u'))} \frac{du'}{a}. \tag{37}$$

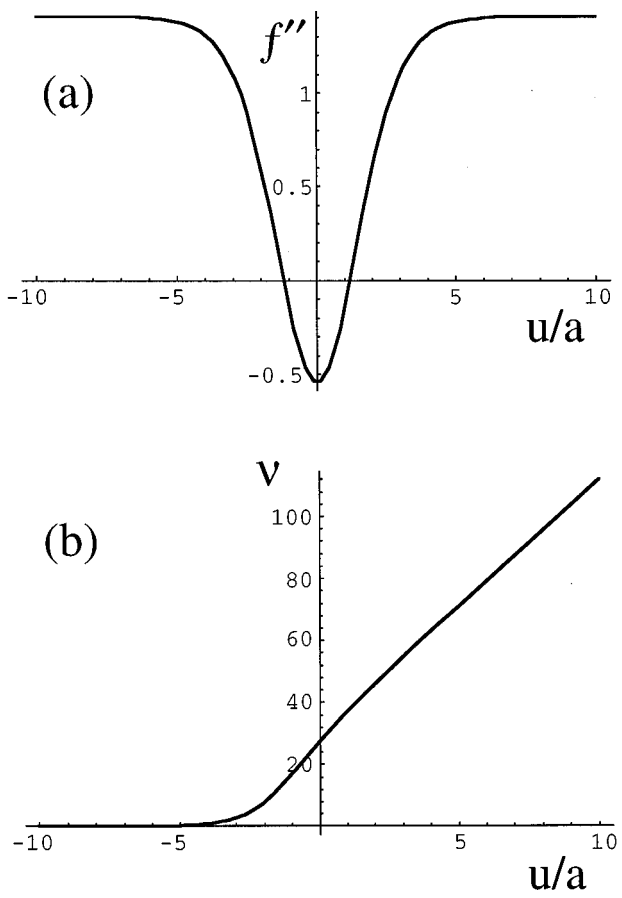

FIG. 3. The ''potential'' $1/\chi[p_0(u)] = f''[p_0(u)]$ (a) and the inhomogeneous term $\nu(u)$ (b) of Eq. (36). Without $\nu(u)$ and the constant term, Eq. (36) is an eigenvalue problem for a particle in the potential well (a).

Without the last two terms, Eq. (36) would be an eigenvalue problem completely analogous to a one-dimensional Schrödinger equation. The ''potential'' $1/\chi[p_0(u)] = f''[p_0(u)]$ and the term $\nu(u)$ are depicted in Fig. 3 [notice that the factor w_0 in the numerator of Eq. (37) cancels out with the prefactor of $M_{\rm loc}$, making $\nu(u)$ dimensionless]. The asymptotes of $\nu(u)$ are readily understood: for $u \to -\infty$, $p_0(u)$ tends towards $p_{\rm eq}^\alpha$, which means that $\nu(u)$ vanishes. On the other hand, for $u \to \infty$, $p_0(u)$ tends to $p_{\rm eq}^\beta$, the mobility becomes constant, and $\nu(u)$ is linear in u. Given this behavior of $\nu(u)$, we see at once that Eq. (36) allows a solution with linear asymptotes: p_1 tends to p_1^α for $u \to -\infty$, whereas for $u \to \infty$, it tends to a straight line with slope m:

$$m = \frac{w_0 \Delta p \chi_{\rm eq}}{a M_{\rm loc}(p_{\rm eq}^\beta)} = \frac{4kT\xi_0^2 \Delta p}{\varepsilon a^3 (1+\Delta p)^2 e^{-z\varepsilon/2kT}}. \tag{38}$$

A brief analysis shows that this expression diverges when T approaches T_c. This is due to the fact that the miscibility gap tends to zero and therefore a very small current is sufficient to drive the interface with high velocity. This shows that the limit $T \to T_c$ is somehow pathological, which is not surprising, as the interface thickness diverges at the critical temperature.

We emphasize that this procedure is valid only near the interface. It is known that the stationary solution for a system

with diffusion and drift (and constant diffusion coefficient) is an exponential; here, we can retrieve only the linear term of this exponential. This means that the solution is limited to regions where $\tilde{v}p_1 \ll 1$, which is the region $u \ll l_D$, where $l_D = D/v$ is the diffusion length. Second, in our model the diffusion coefficient varies with the concentration. But in the linearized equation, it is taken along the equilibrium solution and thus a constant in the bulk phases. This means once again that we must have $\tilde{v}p_1 \ll 1$. This condition limits the velocity range that can be treated for given temperature.

Langer and Sekerka [13] solved their equations by a Green's-function method outside the interface and extrapolated to a hypothetical sharp interface to obtain the corrections to local equilibrium. Here, we have to go beyond this approach because we are precisely interested in the connection between the model parameters, the processes inside the interfacial region, and the resulting kinetic coefficients. To solve Eq. (36), we split up the function $p_1(u)$ in three parts:

$$p_1(u) = p_1^\alpha + g(u) + h(u), \tag{39}$$

where $g(u)$ solves the equation

$$\varepsilon a^2 g''(u) - \frac{g(u)}{\chi_{\mathrm{eq}}} + \nu(u) = 0. \tag{40}$$

The interest of this operation is that if we use for the equilibrium solution $p_0(u)$ the approximation (23), this equation can be solved, and we obtain $g(u)$ explicitly with the aid of a symbolic calculus program. The last remaining piece is $h(u)$, which obeys the differential equation

$$\varepsilon a^2 h''(u) - \frac{h(u)}{\chi(p_0(u))} + \frac{kT(\Delta p)^2[p_1^\alpha - g(u)]}{p_{\mathrm{eq}}^\alpha(1-p_{\mathrm{eq}}^\alpha)\left[1 - 2p_{\mathrm{eq}}^\alpha(1-p_{\mathrm{eq}}^\alpha)\left(\cosh\frac{u}{\xi_0} - 1\right)\right]} = 0. \tag{41}$$

This equation is not directly solvable. To proceed, we use a variational ansatz. The function $h(u)$ is different from 0 only around the origin. We try different test functions and minimize the integral of the square of the left-hand side operator. This is equivalent to the Ritz method in quantum mechanics. $h(u)$ must be orthogonal (in function space) to the function $\tanh'(u/2\xi_0)$, which generates a simple translation of the interface [and has a zero eigenvalue in the eigenvalue problem associated with Eq. (36)]. A candidate that shows good performances is the function

$$h(u) = Au \tanh'\frac{u}{2\xi_0}. \tag{42}$$

Then, p_1^α and A are the variational parameters. We have also tested trial functions with more terms and checked that Eq. (42) gives the dominant contribution. This term corresponds to a modification of the characteristic interface thickness. To see this, note that to first order in $\tilde{v}$, the interface thickness ξ will be

$$\xi = \xi_0 + \tilde{v}\xi_1, \tag{43}$$

where ξ_0 is the equilibrium value (19). If we expand $\tanh(u/2\xi)$ to first order in $\tilde{v}$ using Eq. (43), we find exactly a term of the form (42):

$$p(u) = \frac{1}{2} - \frac{\Delta p}{2}\tanh\frac{u}{2(\xi_0 + \tilde{v}\xi_1)} \approx p_0(u) + \frac{\tilde{v}\xi_1\Delta p}{4\xi_0^2}\, u \tanh'\frac{u}{2\xi_0}. \tag{44}$$

Another way to see that the interface thickness must be different from its equilibrium value is a brief analysis of the solution in region I, that is, the plateau behind the interface. Linearizing Eq. (34) around p_∞^α gives

$$-v\frac{dp}{du} = a^2 M_{\mathrm{loc}}(p_\infty^\alpha)\left(-\varepsilon a^2\frac{d^4p}{du^4} + \frac{1}{\chi(p_\infty^\alpha)}\frac{d^2p}{du^2}\right). \tag{45}$$

We see that this equation is solved by an exponential, $p(u) = p_\infty^\alpha + C\exp(u/\xi)$, if ξ satisfies

$$-\tilde{v} = D_{\mathrm{hom}}(p_\infty^\alpha)\frac{(\xi/a)^2 - \varepsilon\chi(p_\infty^\alpha)}{w_0(\xi/a)^3}, \tag{46}$$

where we have used the identity $D = M/\chi$. For $v = 0$, we retrieve the equilibrium result (19). If ξ was a constant, this equation would furnish a simple relation between v and p_∞^α and allow the determination of p_1^α. Such a simple solution does not correspond to the physical situation: it would mean that we could understand interface-controlled phenomena without any knowledge of what is going on in the interface. Indeed, comparison of Eq. (46) to the simulations shows that we have to allow for a variation of ξ, so that Eq. (46) has three variables, and we cannot directly obtain p_∞^α and ξ as functions of v. On the other hand, the solution obtained by the variational procedure described above substantially implies the processes in the interface via the function $h(u)$ that is localized there.

We therefore choose as variational parameters p_1^α and ξ_1 [using Eq. (42) with $A = \xi_1\Delta p/4\xi_0^2$ from Eq. (44)], which have direct physical meaning. The optimization with respect to these parameters is without problems numerically. We postpone a comparison of the obtained results with our simulations to Sec. VI.

V. DISCRETE SYSTEM

A. Equilibrium states

In our original system, the translational symmetry in space is discrete. But the interface moves continuously in time, and therefore takes all possible positions with respect to the lattice. One could imagine that the interface can be described by some continuous curve as Eq. (23), the points of the lattice system at a time t being given by the values of this function for the points where $x - vt$ is a multiple of the lattice constant a. This is, however, not the case. If we use our evolution equations (17) for a closed system, in which the total mass is fixed to enforce an interface at a given

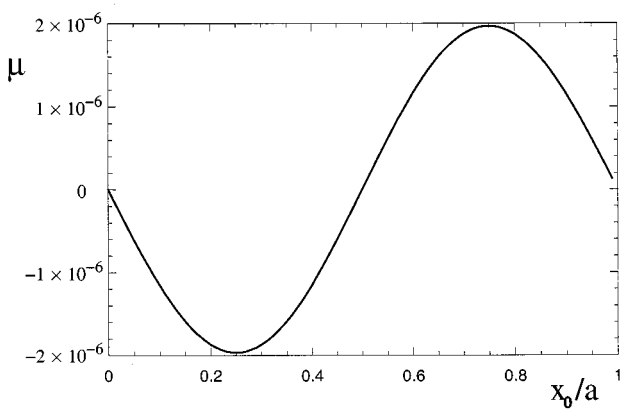

FIG. 4. Plot of the chemical potential μ versus the interface position x_0/a for $T=0.866\,T_c$.

position, the final state is an equilibrium state with constant chemical potential. This equilibrium value of the chemical potential is found to depend on the interface position. In particular, the value $\mu=0$ is taken only for interfaces that are symmetric with respect to a lattice point ($p_{n-k}=\frac{1}{2}-p_k$ for all $k\geqslant 0$ and some fixed n) or with respect to a point in the middle between two lattice points ($p_{n-k-1}=\frac{1}{2}-p_k$). For other interface positions, μ is different from zero in the whole system, which means, in particular, that the bulk equilibrium values (which depend on μ) are slightly modified. This would not happen if we could derive the discrete states from a single continuous curve by off-lattice translations (see [31] for an example of such a situation).

Plotting the chemical potential as a function of the interface position x_0 for an interface in the (10) direction (Fig. 4), we see that $\mu(x_0)$ is nearly a sine:

$$\mu(x_0)=-\mu_c\sin(x_0/a), \tag{47}$$

where μ_c is a constant depending on temperature (Fig. 5) that vanishes near the transition. This behavior is independent on the system size L, as long as $L\gg\xi_0$. As this equation describes lattice effects, we expect μ_c to be a function of the ratio ξ_0/a. The minus sign corresponds to our choice that the x unit vector points into the β phase. We have used the

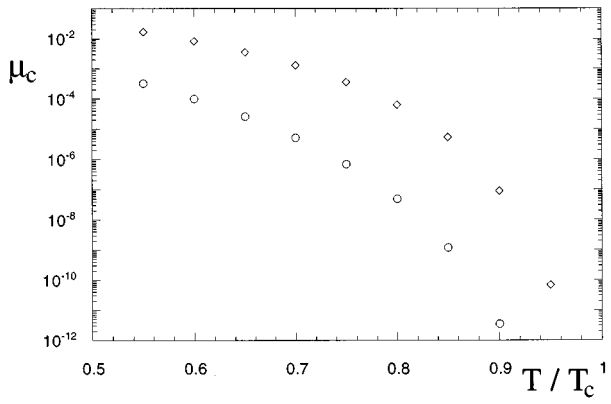

FIG. 5. Critical values μ_c of the chemical potential versus temperature for the main symmetry directions. Diamonds, (10) direction; circles, (11) direction. Note the very rapid decay for $T\to T_c$.

method of the Gibbs dividing surface to define the interface position: the interface profile is replaced by a step, containing the same mass as the original system. Then the kink position x_0 is determined by the equality

$$x_0p_0+(L-x_0)p_L=\sum_{i=0}^{L}p_i\,. \tag{48}$$

The sinelike behavior is verified in a large range of temperature. To gain a deeper understanding of this phenomenon, we use the theory of area-preserving maps as applied to mean-field interfaces by Pandit and Wortis [22].

To find the discrete equilibrium states, we have to solve the equation $\mu_k=\mu=\text{const}$ for all k, using the discrete expression (8) for the chemical potential. For an interface in the (10) direction, this equation can be rewritten as a two-dimensional mapping, setting $x_k=p_{k-1}$ and $y_k=p_k$:

$$x_{n+1}=y_n\,,$$

$$y_{n+1}=-\mu/\varepsilon+2y_n-x_n-z(y_n-\tfrac{1}{2})+kT/\varepsilon\,\ln\frac{y_n}{1-y_n}\,. \tag{49}$$

The Jacobian of this mapping is 1: it is area preserving. It has two fixed points, corresponding to the two equilibrium concentrations. An interface solution is a series of iterations of this mapping, connecting the two fixed points. As remarked by Pandit and Wortis, unlike the continuum version, which possesses a unique heteroclinic orbit connecting the two fixed points, the discrete mapping (49) has chaotic properties. This can be seen if we plot the inset of one of the fixed points, which is the set of all points that will be mapped onto the fixed point after an infinite number of iterations of the mapping (49). It has the structure of a chaotic trajectory, passing in the vicinity of the other fixed point infinitely often without ever reaching it. The outset of the other fixed point can be constructed by symmetry: it is the set of all points that will flow to the fixed point under (infinite) iteration of the inverse mapping. An interface solution, which has to connect the two fixed points, is a set of points that belong simultaneously to the outset of one fixed point and to the inset of the other. For $\mu=0$, the phase portrait is symmetric [Fig. 6(a)], and the intersection points of inset and outset form two such sets, corresponding to interfaces that are symmetric with respect to a plane and to a half plane: we recover the result of our simulations. In Fig. 6(b) we depict a phase portrait for a small positive value of μ. We see that inset and outset deform, and the intersection points move: the two solutions approach each other. For some critical value, which is identical to μ_c defined in Eq. (47), the solutions coincide, and beyond, no interface solution is possible [Fig. 6(c)]. In real space, this motion of the intersection points corresponds to a displacement of the interface: the first solution moves to the right, whereas the second moves to the left; at the critical value of μ, they meet. The antisymmetry of Eqs. (49) with respect to an exchange of particles and holes assures that the inverse motion takes place when μ is negative. We thus recover the dependence of μ on the interface position. From the structure of the orbits in the phase portrait, we can deduce that the function

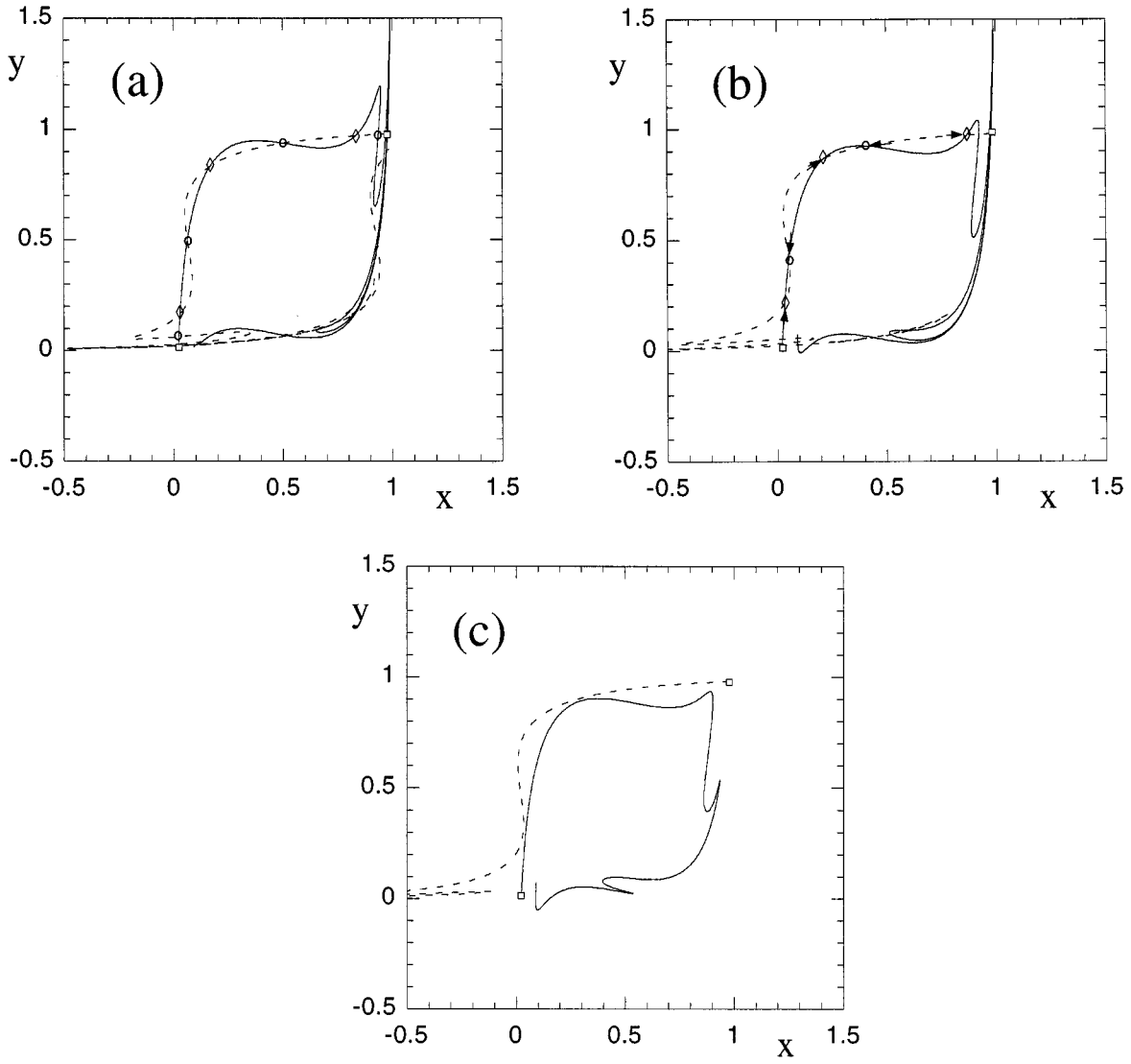

FIG. 6. Phase portraits of the (10) interface for $T=0.5T_c$ and $\mu=0$ (a), 0.02 (b), and 0.04 (c). We show the beginnings of the outset of the β-phase fixed point (solid line) and of the inset of the α-phase fixed point (dashed line). A point (x,y) in this phase portrait is equivalent to a couple of concentrations (p_k, p_{k+1}). Some points forming the two interface solutions are marked by diamonds and circles. In the vicinity of each fixed point (marked by open squares) there are infinitely many such intersection points (not shown). The arrows in (b) indicate in which direction the interface points have moved in comparison to (a). All diamonds have moved upwards and to the right, whereas the circles have moved downward and to the left. In (c), the interface solutions have ceased to exist. Notice that this figure is nearly identical to Fig. 5 of Ref. [22]. See that paper for more details on this kind of diagrams.

$\mu(x_0)$ is periodic, antisymmetric with respect to lattice points, linear with finite slope around the lattice points, and has horizontal tangents at its extremal values. The simplest such function is the sine of Eq. (47). It would be desirable to calculate μ_c directly from the properties of the chaotic map; however, this seems a difficult task. The fact that μ_c is intimately related to the structure of the mapping is illustrated by a comparison between the two symmetry directions. In the (11) direction, the mapping equivalent to Eqs. (49) reads

$$x_{n+1}=y_n,$$

$$y_{n+1}=-\mu/2\varepsilon+2y_n-x_n-\frac{z}{2}\,(y_n-\tfrac{1}{2})+\frac{kT}{2\varepsilon}\ln\frac{y_n}{1-y_n}. \tag{50}$$

This seems to be not very different from Eqs. (49); however, in this direction the sign of the sine is inverted, and μ_c is two orders of magnitude smaller than in the (10) direction (see Fig. 5). Visualizing the phase portrait [Fig. 7(a)], we see that for the same temperature, the trajectories seem to be much less chaotic. To see the intersections between inset and outset, we have to magnify a part of the phase portrait [Fig. 7(b)]. Such chaotic behavior seems to be a general feature of discrete mean-field equations. However, results have been reported on a discrete but integrable system of a similar kind [31], but in this model a chemical potential cannot be uniquely defined.

The variations of μ are accompanied by variations of the surface tension. Pandit and Wortis already remarked that of the two solutions at $\mu=0$, the one with off-plane symmetry, has a lower surface tension. In the (11) direction, this situa-

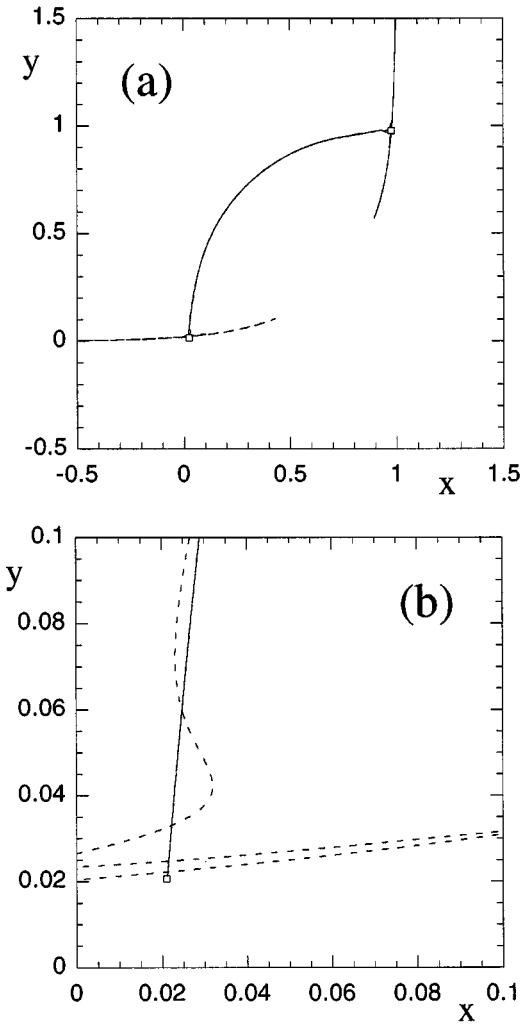

FIG. 7. Phase portrait of the (11) interface at $T=0.5T_c$ and $\mu=0$ (a). Only the beginnings of inset and outset are shown, hence the apparent asymmetry of the diagram. To see the structure of inset and outset, one has to magnify a part of this diagram (b): the (11) interface is ''less chaotic'' than the (10) interface. The open squares indicate the fixed points.

tion is inverted. If we calculate numerically the surface tension for the different equilibrium states, we find to a good precision

$$\sigma(x_0)=\frac{\sigma_1+\sigma_2}{2}+\frac{\sigma_1-\sigma_2}{2}\cos(x_0/a), \tag{51}$$

where σ_1 and σ_2 are the surface tensions of the two symmetric ($\mu=0$) solutions. This determines the behavior of the system during equilibration. For an infinite system, matter can be redistributed to infinity, and the interface will always relax to the position of lowest surface tension, which has zero chemical potential. If the system has finite size, it equilibrates at the state with lowest surface tension compatible with the constraint of constant mass. It is in this situation that we can observe the states at intermediate position. But even in finite systems, we have a slight redistribution of mass, because the equilibrium concentrations depend on the chemical potential, so that we cannot simply use the total mass to define the interface position: the only correct choice is the method of the Gibbs dividing surface (48).

B. Stationary states

We have seen in Sec. V A that quantities as the equilibrium chemical potential and the surface tension of a planar interface depend on its position relative to the lattice. An interface that is forced to advance by a constant current injected into the system therefore generates oscillatory behavior. Mathematically, this stems from the fact that unlike in continuous systems, where a stationary state $p(x-vt)$ satisfies $\partial p/\partial t=-v\,\partial p/\partial x$, in a system with discrete translational symmetry the set of concentrations $p_n(t)$ satisfies

$$p_n(t)=p_{n-1}(t-a/v), \tag{52}$$

where v is the (constant) stationary velocity. However, time is continuous. Therefore, we could rewrite the evolution equation (17) using the condition (52) as an ordinary differential equation for the continuous time variable t. Unfortunately, this equation is nonlocal in time and thus not easier to solve. However, we can visualize the stationary state as a continuous curve, tracing the trajectory of a point $p_n(t)$, while it traverses the interface. For high temperatures this trajectory tends to the continuous stationary state that we have determined in Sec. IV; when one lowers the temperature, oscillations appear, which we will analyze now.

For small velocities, the interfacial region (region II of Fig. 2) is slightly modified, but keeps its overall shape. It stays close to the equilibrium shape, and monitoring the dynamics we see that the chemical potential in this region oscillates with the advance of the interface, as for the equilibrium states (see Fig. 11 below). So it seems that for small driving forces the relation (47) stays valid: the chemical potential oscillates with the spatial periodicity of the lattice and the frequency $v/a=w_0\tilde{v}$. Currents are driven by chemical potential gradients, so these oscillations can modify the behavior of the whole system. Seen on the scale of the macroscopic sharp-interface models, this is like an oscillating boundary condition at the interface.

Let us analyze the effect on the dynamics in the bulk phases. First, we discuss what is happening in the α phase behind the interface (region I). To this end we linearize the full discrete equation of motion (17) around the limit value p_∞^α. Writing $p_k=p_\infty^\alpha+\delta_k$, we obtain to first order in δ_k,

$$\frac{d\delta_k}{dt}=M_{\rm hom}(p_\infty^\alpha)[f''(p_\infty^\alpha)(\delta_{k-1}-2\delta_k+\delta_{k+1}) -\varepsilon(\delta_{k-2}-4\delta_{k-1}+6\delta_k-4\delta_{k+1}+\delta_{k+2})]. \tag{53}$$

Assuming, as before, an exponential behavior, $\delta_k \propto \exp[q(ka-vt)]$, this gives the following equation for q:

$$-\frac{v}{D_{\rm hom}(p_\infty^\alpha)}\,q=(e^{aq}-2+e^{-aq})[1-\varepsilon\chi(p_\infty^\alpha) \times(e^{aq}-2+e^{-aq})]. \tag{54}$$

This is the discrete analog of Eq. (46). But in contrast to Eq. (46), which always has three real solutions, Eq. (54) is a transcendental equation that may have a multitude of solu-

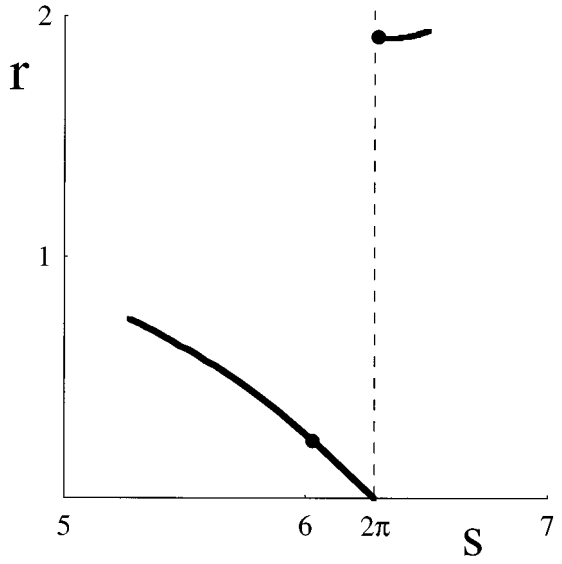

FIG. 8. Image of a part of the (s,r) plane to show some of the solutions of Eq. (55) for $T=0.7T_c$. The points are the solutions of Eq. (55) for $T=0.7T_c$, $\tilde{v}=6.074\,437\times10^{-5}$, and $p_\infty^\alpha=0.913\,610\,8$ ($j_0=5\times10^{-5}$). The corresponding nonoscillating solution is at $s=0$, $r=1.911\,01$. The lines are drawn using the numerical value $p_1^\alpha=-12.329$ and velocities ranging from 0 ($s=2\pi$) to 10^{-3}. Similar patterns are seen around multiples of 2π.

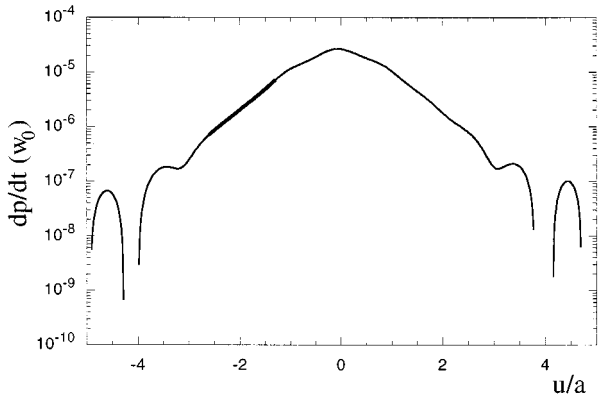

FIG. 9. Time derivative (measured in units of w_0) of a point fixed in space as the interface passes by, on a logarithmic scale, for $T=0.7T_c$ and $j_0=5\times10^{-5}$. Behind the interface, there is a region where the decay is exponential (thick line segment). This region is too small to get results of sufficient precision. In addition, it is too near the interface for the linearized equation (53) to be valid. To both sides of the interface, we see the onset of oscillations. The missing line segments are regions where the time derivative is negative.

tions, in particular, complex ones that correspond to oscillating behavior. Writing $aq=r+is$, with r and s real, we arrive at the following couple of real equations:

$$-\frac{\tilde{v}w_0}{D_{\rm hom}(p_\infty^\alpha)}\,s=2\,\mathrm{sins}\,\mathrm{sinh}r[1-4\varepsilon\chi(p_\infty^\alpha)\times(\mathrm{coss}\,\mathrm{cosh}r-1)],$$

$$-\frac{\tilde{v}w_0}{D_{\rm hom}(p_\infty^\alpha)}\,r=2(\mathrm{coss}\,\mathrm{cosh}r-1)+4\varepsilon\chi(p_\infty^\alpha)\times[\sin^2 s\,\sinh^2 r-\cos^2 s\,\cosh^2 r+1], \tag{55}$$

which have to be solved for r and s. As in the continuum case, for $v=0$ we recover the equilibrium situation. For arbitrary v, we see that $s=0$ always solves trivially the first equation, and we are left with one equation for r. This is a branch of nonoscillating solutions. Other solutions that give negative values for r have to be discarded. However, there are branches with positive r for nonzero values of s: when the ratio $\tilde{v}w_0/M$ is small, these solutions appear in pairs, with s near a multiple of 2π, one slightly smaller, one slightly bigger. This corresponds to damped oscillator solutions that have a wavelength $\lambda=2\pi a/s$ nearly equal to a harmonic of the lattice and a decay length a/r. In Fig. 8. we show for one particular value of the parameters $\tilde{v}$ and p_∞^α the possible solutions (r,s) near $s=2\pi$. Using the numerical value for p_α^1, we can also trace the approximate form (to linear order in $\tilde{v}$) of the branches of solutions for small $\tilde{v}$. Around other multiples of 2π, the picture is similar. The family of solutions with s slightly above the multiples of 2π have decay lengths very near the equilibrium solution, whereas for the other family r goes to 0 as $\tilde{v}$ vanishes, which means a diverging decay length.

Which of these solutions will be selected? Equation (53) is linearized in p, so we could even expect a superposition of several solutions. Now consider the oscillations at the interface: the concentration behind the interface behaves like a damped oscillator, which evolves between a fixed value at $-\infty$ (frequency 0) and an oscillating concentration which is ''dragged'' by the moving interface. The two solutions, which will play obviously the most important role, are the nonoscillating solution and the one with the first nonzero value of s, slightly below 2π. To check this assertion with our numerical simulations, it is best to plot the time derivative of one point (fixed in space) while the interface advances. The nonoscillating solution decays much faster (smaller decay length), and even if it is predominant directly behind the interface, farther behind the oscillating part will show up. Indeed, plotting dp/dt on a logarithmic scale shows a region behind the interface with exponential decay, giving a straight section in the plot, and the onset of oscillations behind (Fig. 9). Magnifying these oscillations, we see the damped oscillator, and we can extract the corresponding values of r and s. An example is shown in Fig. 10: the agreement with the predictions from Eq. (55) is excellent.

Now we have to remember that in our system time is continuous, but space is discrete. If we look at the spatial dependence for some time t, we see slow variations: because of the lattice structure, wave vectors differing by 2π are equivalent. We define $\varphi=2\pi-s$. The apparent wavelength of the undulations is then $\lambda'=2\pi a/\varphi$ and beatings occur. This is shown by open circles drawn in Fig. 10 at distances corresponding to a lattice constant. When $\tilde{v}$ approaches 0, a leading order expansion of Eq. (55) gives that $\varphi=r$ (note the slope -1 of the concerned branch in Fig. 8) and

$$r=\varphi=\sqrt{\pi\tilde{v}w_0/D_{\rm hom}(p_\infty^\alpha)}=\sqrt{\pi a/l_D} \tag{56}$$

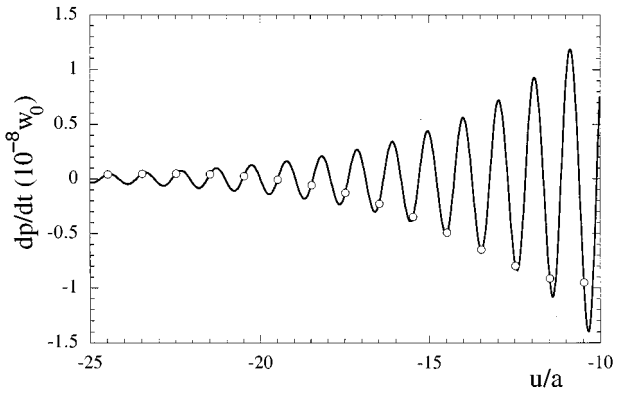

FIG. 10. Same as Fig. 9, but farther behind the interface and seen on a linear scale. A fit with a damped sine is indistinguishable from the curve and gives $s=6.0288$ and $r=0.2424$, whereas the predictions from Eq. (55) are $s=6.028\,11$, $r=0.2414$. Open circles are drawn at distances corresponding to one lattice step. This illustrates the beatings discussed in the text.

($l_D=aD/w_0\tilde{v}$ is the diffusion length). λ' and the decay length diverge, keeping always the same ratio. The frequency $s\tilde{v}w_0$ goes to 0 linearly in $\tilde{v}$, and thus the phase velocity vs/r behaves like $\tilde{v}^{1/2}$.

This behavior can be readily explained in terms of diffusion. The variations of the chemical potential at the interface cause variations in concentration, of the order of $\chi_{\rm eq}\mu_c$ [this follows from the fact that, for small μ, $p-p_{\rm eq}=\mu\chi_{\rm eq}$, and using Eq. (47)]. Imagine an initially homogeneous phase. When the interface moves, it creates in its wake a perturbation that causes a diffusive flux: the perturbation propagates. The characteristic length scale is the diffusion length l_D, the characteristic time scale is a^2D/v^2. When v tends to 0, the diffusion length diverges, implying that the length scales of the problem grow, but the diffusion time diverges even faster. Transport over the length scale of the diffusion length (which is necessary to propagate the wave) is very slow, which explains the behavior of the phase velocity. When the interface velocity grows, the diffusion length decreases, and the time necessary to equilibrate the fluctuations becomes comparable to the inverse frequency of the oscillations: they are damped very rapidly.

To summarize, in the wake of the interface, we find damped oscillations of density and current which can have wavelengths considerably larger than the lattice constant, especially for slow velocities, where, in addition, the decay length becomes big. However, their amplitude is small (of order $\chi_{\rm eq}\mu_c$), so it should be difficult to observe such a phenomenon experimentally. In addition, we do not know precisely whether the mean-field approximation mimics correctly the progressive filling of the atomic layers at low temperatures, where such oscillations become stronger. A similar phenomenon has been reported in the context of kinetic stochastic growth models [25,26]. The authors observed oscillations in the density of a growing aggregate, due to the discrete lattice structure. Note, however, that the physical context is different, because this work does not take into account relaxation processes, so there is no diffusion and the density variations are ''frozen'' once the interface has passed. In addition, their system was not limited by diffusion. But it is interesting to note the similarities: oscillations arise because an interface advances continuously in a lattice model. We believe that such oscillations are a general feature of deterministic discrete growth equations (see also [27]), but in real systems they should be masked by fluctuations, absent in our mean-field approach.

On the other side of the interface, in region III, the situation is quite different because of the presence of the driving current. In this region, too, the oscillations of the chemical potential at the interface have important effects. If we fix the chemical potential at some (large) distance of the interface, variations of μ at the interface imply variations of the chemical potential gradient, and thus of the flux. A similar effect is observed when we fix the current: when the chemical potential at the interface increases, the chemical potential in all the region in front of the interface must increase to maintain a gradient towards the interface. The only way to achieve this is to ''stack'' some matter, because in region III, μ is an increasing function of the concentration. Matter accumulates in front of the interface and is ''liberated'' when the chemical potential at the interface decreases, causing a strong flux towards the interface. Hence we conclude that the oscillations of the chemical potential cause fluctuations in the current arriving at the interface.

But this means, because of mass conservation, that the interface velocity varies. The variations of the incoming flux cannot be compensated by the outgoing flux behind the interface, the latter being much smaller than the former. We can indeed observe directly fluctuations of the growth velocity. However, we have to be careful, because a proper definition of the interface velocity is difficult. Out of equilibrium, the profile is not symmetric any more and we cannot separate ''interface'' and ''ramp'' profile: the application of the Gibbs dividing surface method is impossible. We can define the interface position by the symmetric point, $p=\frac{1}{2}$. But alternate definitions are possible, for example, the inflection point. As we have shown that the interface shape depends on velocity, neither of these definitions can claim superiority; however, the differences are small. We will adopt the first definition, operationally the simplest one. Our interface being defined on a lattice, we need an interpolation procedure to determine this position for arbitrary time. A comparison at equilibrium to the Gibbs method shows that a simple linear interpolation introduces rather large errors; the best procedure seems to be a tanh interpolation, which gives (to very good precision at high temperatures, to some percents at $T=0.5T_c$) the same results as the Gibbs method at equilibrium. We have plotted in Fig. 11 the interface velocity (the time derivative of the interface position) during several cycles. We also have displayed the variations of chemical potential and of the current arriving at the interface (having measured some sites in front of the interface position). The periodic fluctuations are clearly visible. The amplitude of the oscillations of the chemical potential is in good agreement with the equilibrium value μ_c. The ''zero line'' of the sine function is shifted to a small positive value, but the symmetric points are still on lattice planes or half planes. Note the phase relationship between chemical potential and velocity: the interface is fastest when the slope of the chemical potential curve is steepest. If we consider the surface tension (51), we see that it is in phase with the velocity, that is, the

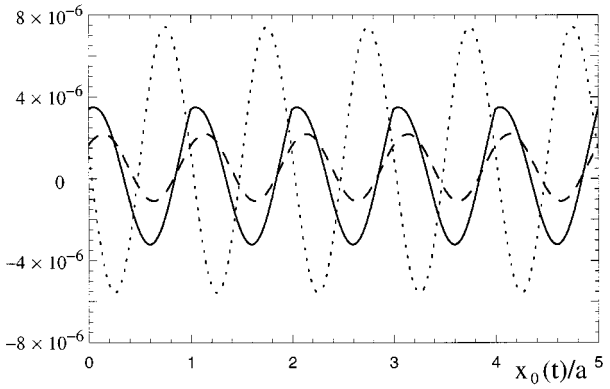

FIG. 11. Difference between instantaneous interface velocity and its mean (solid line), difference between instantaneous current some sites in front of the interface and j_0 (dashed line), and chemical potential at the interface (dotted line) versus the interface position $x_0(t)/a$, for $T=0.73T_c$ and $j_0=5\times10^{-5}$. The chemical potential has been divided by 100 to show the three curves on the same scale. The mean velocity is 6.33×10^{-5}; thus the relative amplitude of the oscillations is about 6%.

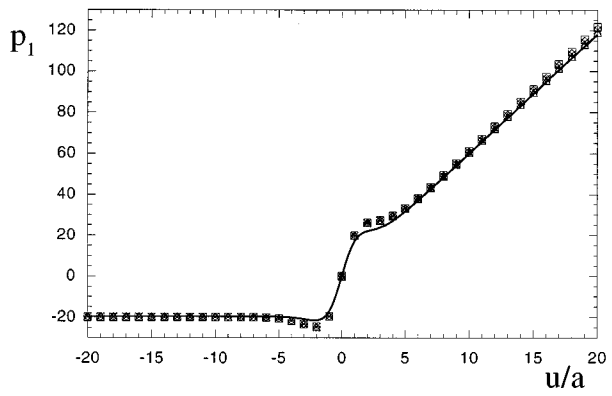

FIG. 12. Linear part of the shape correction p_1, at $T=0.86T_c$, as determined by simulations (symbols) for velocities $\tilde{v}=(0.668\,07, 1.3390, 2.0129, 2.6899, 3.3701)\times10^{-5}$ and by the continuum approximation (solid line).

interface is fastest at the points of highest surface tension. This contradicts the somewhat naive assumption put forward in our previous paper [21] that the interface should slow down when it has to ''climb'' a hill of surface tension. Here we see that the dynamics is accurately described in terms of the chemical potential, whereas simple static considerations lead to wrong interpretations. The slight phase difference between velocity and current is due to the fact that the current is measured some sites in front of the interface.

It is probably impossible to observe directly these fluctuations, because a definition of an interface position on an atomic scale and even more its measurement seem impossible. However, the oscillations of chemical potential and current could be observable. Note, on the other hand, that we have not taken into account thermal noise: in any ''real'' system it should destroy the weak coherent oscillations at a small distance of the interface.

VI. RESULTS

We will now summarize our main results and compare the continuum approximation to the simulations. First, let us comment on the validity of our linearized ansatz (35) and the quality of the continuum approximation. In Fig. 12, we show a data collapse for $T=0.86T_c$, that is, we plot the difference between stationary state and equilibrium profile as obtained numerically, divided by the velocity. If the linear hypothesis is true, all points should fall together. We see that this is indeed the case. The slight differences for larger positive u are traces of higher-order terms: for $p_1>100$ and $\tilde{v}>10^{-5}$, $\tilde{v}p_1$ is no longer small enough for the linear approximation to be strictly valid. If we extrapolate in this region the slope of the different curves to $\tilde{v}=0$, the agreement with the value m given by Eq. (38) is excellent. The solid line is the prediction of the continuum approximation. All qualitative features of the shape correction are well reproduced, even if there are small differences in the interface. We emphasize that this curve is not a fit to the data points but the direct result of the variational procedure discussed in Sec. IV.

In Fig. 13, we compare the results of the continuum approximation with numerical results for the solute trapping coefficient p_1^α. The results are very good for a large range of temperatures. Evidently, the continuum method cannot describe the differences between the (10) and (11) directions. However, these differences are small for high temperatures and decrease to 0 when $T\to T_c$. Towards $0.5T_c$ the data points for the (10) direction differ appreciably from the theoretical curve, whereas for the (11) direction the agreement stays very good. This reflects once more the ''more chaotic'' nature of the (10) interface.

In Fig. 14, we show ξ_1 in function of temperature, divided by $\xi_0^4(T)$. Near the critical temperature, ξ_1 can be well approximated by

$$\xi_1 = C\xi_0^4, \tag{57}$$

where the coefficient was numerically determined to be $C=102.3$. Unfortunately, reliable numerical values for ξ_1 are

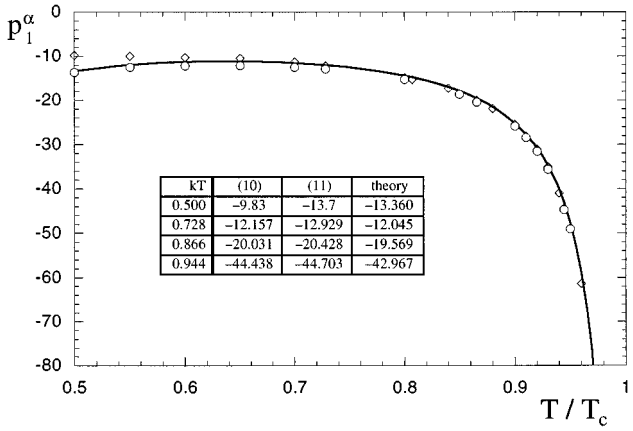

FIG. 13. Plot of the ''Solute trapping'' coefficient p_1^α versus temperature. The solid line is the continuum approximation, symbols are values of numerical simulations. Diamonds, (10) direction, circles, (11) direction. Inset: table with some numerical values of p_1^α.

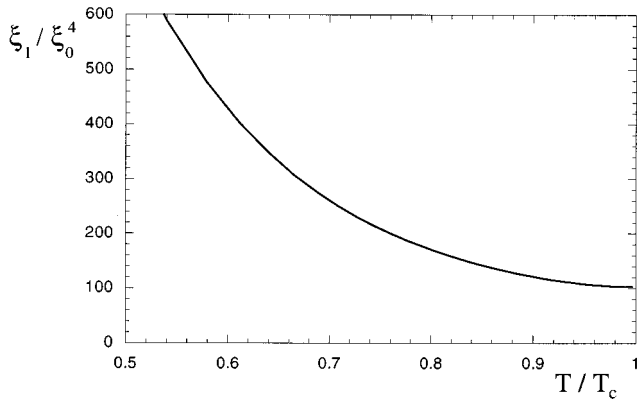

FIG. 14. Plot of ξ_1/ξ_0^4 versus temperature. The horizontal tangent at T_c shows that the asymptotic behavior of ξ_1 is like ξ_0^4.

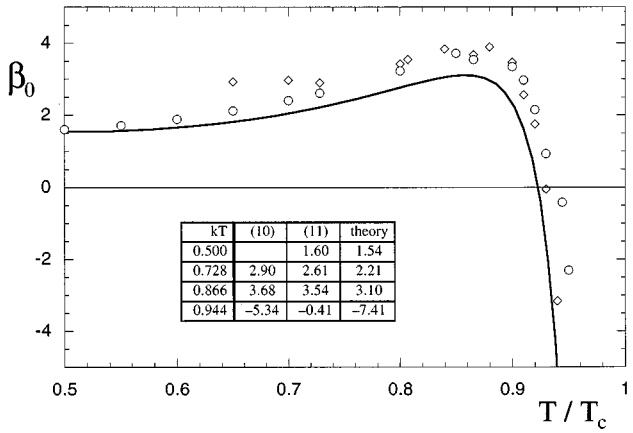

FIG. 15. Kinetic coefficient β_0 versus temperature. Symbols as in Fig. 13. Inset: table with some numerical values of β_0.

difficult to obtain. As shown in Fig. 9, the region behind the interface in which the decay length ξ can be measured is too small to get a sufficient precision. To determine ξ_1 for (typical) dimensionless velocities of the order 10^{-5}, we would need a precision of four digits at least on ξ. For higher temperatures, above all in the (11) direction, the situation is somewhat better than depicted in Fig. 9, because the exponential decay region is larger; it permitted us to verify that ξ_1 is of the correct order of magnitude. Hence we conclude that this approximation is a valuable tool to investigate interface dynamics over a quite large range of temperature, even if the condition $\xi_0 \gg a$ is not strictly satisfied (at $0.5T_c$, $\xi_0 \approx 0.25a$).

p_1^α and ξ_1 diverge when we approach the critical temperature. This reflects the singular nature of this limit, which was already discussed in Sec. IV: the interface becomes very extended in space and the miscibility gap very small. Thus a very small current can cause large deformations of the interface shape. At the critical temperature, the interface disappears, so it is normal that there appear singularities in the ''shape correction.'' For temperatures lower than $0.5T_c$, the diffusion in the α phase becomes so slow that the linear regime is valid only for very small velocities. Here, we can attain very easily the nonlinear regime. In this limit, the interface is very sharp, nearly a step profile, and our model becomes rather similar to the phenomenological model for solute trapping proposed by Aziz [9]. In this model, growth takes place by activated jumps of atoms through a (sharp) interface. It would be interesting to investigate more in detail this limit. To summarize, we have a region approximately between $0.5T_c$ and $0.95T_c$, which is described correctly by the linear continuum approximation. In this region, the interface becomes more ''rigid'' when the temperature goes down, that is, one needs a stronger driving force to cause appreciable deformations of the interface profile.

Once the two parameters p_1^α and ξ_1 are determined, we can obtain other quantities of interest. The kinetic coefficient β_0 used in the dynamical extension of the Gibbs-Thomson condition valid to linear order in $\tilde{v}$ is defined by the relation

$$\frac{p_{\rm int}^\beta - p_{\rm eq}^\beta}{\Delta p} = \beta_0 \tilde{v}, \tag{58}$$

where $p_{\rm int}^\beta$ is the concentration immediately ahead of the moving interface. To get this concentration, we choose once more the point $p=\frac{1}{2}$ as definition of the interface position and extrapolate from the ramp profile. In the simulations, we have to take care of the oscillations in front of the advancing interface. We fitted a straight line after every iteration step, determined its intercept, and averaged over one period. Except for low temperatures in the (10) direction, this procedure gave satisfying results. After subtraction of the equilibrium concentration, the resulting concentrations were divided by $\tilde{v}$, and extrapolation to $\tilde{v}=0$ gives β_0. In the continuum approximation, it is sufficient to determine the asymptotic straight-line fitting to p_1 in region III; its intercept at $u=0$ gives directly $\Delta p \beta_0$. The results are plotted in Fig. 15. The agreement between simulations and continuum approximation is not as good as for p_1^α, but the overall shape of the curve is well reproduced. The most prominent feature is a change of sign of the kinetic coefficient: near the critical temperature, it becomes negative. This prediction of the continuum approximation (line) is confirmed by the simulations (data points). A negative β_0 seems at first glance very strange, as usually the kinetic coefficient is associated with attachment kinetics and hence a free-energy dissipation at the interface, which has to be always positive. A look on the analytic expressions can help us further. In region III, the correction $h(u)$ in Eq. (39) falls off to zero very rapidly. We need only consider the asymptote of $g(u)$. Using its explicit expression, we find for its intercept g_0:

$$g_0 = 2m\xi_0 \Delta p \left(\frac{T_c}{T} + \frac{1}{1-\Delta p} \right), \tag{59}$$

where m is given by Eq. (38). This term is always positive and diverges for $T \to T_c$. But we have also to take care of the constant term in Eq. (39): the whole profile is shifted by p_1^α. With definition (58), β_0 is given by

$$\beta_0 = \frac{g_0 + p_1^\alpha}{\Delta p} = 2m\xi_0 \left(\frac{T_c}{T} + \frac{1}{1-\Delta p} \right) + \frac{p_1^\alpha}{\Delta p}. \tag{60}$$

Now, p_1^α is negative and diverges near T_c. So the kinetic coefficient is the sum of two divergent terms of different sign, and the negative sign wins near the critical temperature.

This explains in part the distance between data points and prediction in Fig. 15: small errors in p_1^α can produce large relative errors in β_0. This leads to stronger differences between the two directions; however, the form of the β_0 curve is quite the same.

Physically speaking, we have a connection between solute trapping and the kinetic concentration shift. The chemical potential behind the interface is always lowered by the solute trapping effect. For low temperatures, this is compensated by the chemical potential difference through the interface, leading to a positive chemical potential in front of the interface and a positive β_0. Near the critical temperature, the solute trapping effect becomes so strong that this compensation is no longer fully possible: the chemical potential (and hence the concentration) is lowered even in front of the interface, leading to a negative β_0. But the chemical potential difference across the interface stays positive, leading to a positive free-energy dissipation. In the conventional equations of dendritic growth, diffusion and solute trapping in the solid are usually neglected: then, β_0 is always positive. Notice also that the sign change takes place only quite near the ''pathological'' limit $T \to T_c$.

Further insight can be gained considering the interface mobility. It is defined by

$$\tilde{v} = M_I \Delta\mu, \tag{61}$$

where $\Delta\mu$ is the chemical potential difference between the two sides of the interface. This relation describes the resistance of an interface against the driving force, resulting from incorporation kinetics. Using once more the two straight line asymptotics of $g(u)$, we can calculate the chemical potential difference as extrapolated to a sharp interface. Is is evidently linear in $\tilde{v}$, and the proportionality constant is

$$M_I = \frac{a M_{\mathrm{loc}}(p_{\mathrm{eq}}^\beta)}{2 w_0 (\Delta p)^2 \xi_0 \left(\dfrac{T_c}{T} + \dfrac{1}{1-\Delta p} \right)}, \tag{62}$$

always positive. This expression can be obtained in another way by the following considerations. The chemical potentials on the two sides of the interfaces are $\mu(p_{\mathrm{eq}}^\alpha + \tilde{v} p_1^\alpha)$ and $\mu(p_{\mathrm{eq}}^\beta + \tilde{v}\Delta p \beta_0)$, respectively. Linearizing these expressions in $\tilde{v}$ leads to the following relations between the linear coefficients:

$$M_I = \frac{\chi_{\mathrm{eq}}}{\Delta p \beta_0 - p_1^\alpha} = \frac{\chi_{\mathrm{eq}}}{g_0}. \tag{63}$$

This shows the connection between the three coefficients: In Fig. 16, we plot the theoretical prediction (62) (full line) and simulation data, using our values of p_1^α and ξ_1 and the formula (63). The agreement is very good; slight scattering at high temperatures comes from the fact that higher-order terms in $\tilde{v}$ are increasing, and the extrapolation for β_0 becomes less accurate. The anisotropy between the two directions is small.

Let us finally discuss the relation between interface velocity and the current crossing the interface. In a sharp interface model, mass conservation implies

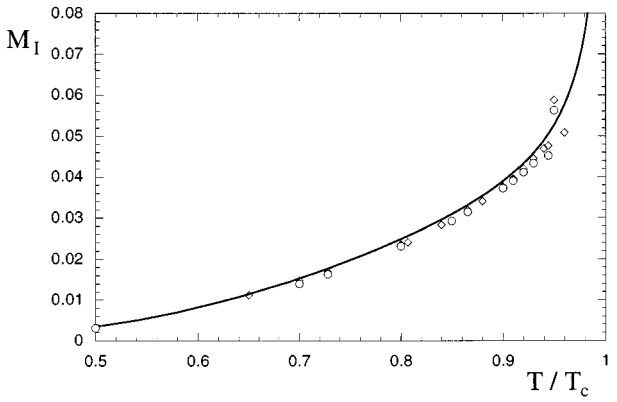

FIG. 16. Interface mobility M_I versus temperature. Symbols as in Fig. 13.

$$j_{\mathrm{int}} = -w_0 \tilde{v} (p_{\mathrm{int}}^\alpha - p_{\mathrm{int}}^\beta), \tag{64}$$

where j_{int} is the current crossing the interface, and the p_{int} are the concentrations in the α and β phase immediately adjacent to the interface. In our case, mass conservation is guaranteed by Eq. (32). Using this equation with the extrapolated concentration in the β phase, $p_{\mathrm{eq}}^\beta + \tilde{v}\Delta p \beta_0$, we obtain

$$\begin{aligned} j_{\mathrm{int}} = j(0) &= -w_0 \tilde{v} (p_{\mathrm{eq}}^\alpha + \tilde{v} p_1^\alpha - p_{\mathrm{eq}}^\beta - \tilde{v}\Delta p \beta_0) \\ &= -w_0 \tilde{v} \Delta p + w_0 \tilde{v}^2 \frac{\chi_{\mathrm{eq}}}{M_I}. \end{aligned} \tag{65}$$

This is the first-order correction to the zeroth-order expression $j = -w_0 \tilde{v} \Delta p$, which corresponds to an advancing interface in local equilibrium.

VII. CONCLUSION

We have calculated stationary interface shapes starting from an isothermal lattice gas model. Despite its simplicity, this model displays several phenomena observed in experiments, as solute trapping and a kinetic shift of local equilibrium at the interface. Using a continuum approximation, we can calculate the corresponding coefficients to linear order in the velocity, starting from the microscopic interaction between the particles. This approximation involves a variational procedure with respect to two parameters that are related to solute trapping and to the interface thickness, which is a function of velocity. Comparison to simulations showed that this approximation is valid over a wide range of temperature. It gives the concentration of the growing phase and the concentration ahead of the growing front. This allows us to establish a relation between interface velocity and the current crossing the interface.

We found that solute trapping and the kinetic concentration shift are related in this linearized theory, leading to a change of sign in the kinetic coefficient near the critical temperature. Solute trapping and kinetic coefficient are related to the interface mobility by relation (63). It would be interesting to verify this relation experimentally.

With the (relative) exception of the kinetic coefficient β_0, the agreement between simulations and continuum theory is very good. This approach does not allow us to

predict the anisotropy of the coefficients. It was found to be small, once again with exception of β_0 in a certain range of temperatures. Near the critical temperature, all coefficients diverge, showing the pathological nature of this limit, in which a well-defined interface ceases to exist.

Furthermore, we have shown that oscillations of growth velocity and chemical potential occur due to the discrete nature of the model (existence of a crystalline structure, or of a host lattice) and the coupling between interface and diffusion field. There also exist damped density waves in the wake of the interface. Such oscillations seem to be a general feature of mean-field-like growth models. Neither of these effects should be simple to observe in a real experiment, because of the small amplitude of the oscillations and the presence of thermal noise.

Starting from a microscopic model, we have achieved a complete understanding of the dynamics of a planar interface in a mean-field approximation, going beyond the known phenomenological and mesoscopic theories, which do not specify detailed microscopic dynamics. The choice of the initial model is not restrictive: the methods we have presented are flexible enough to be applied to lattice gases with more complex interactions, thus opening the way to investigate the relation between microscopic interactions and macroscopic interface kinetics.

It would be interesting to obtain similar results in a true stochastic model, or improve on the simple mean-field theory using more sophisticated schemes to devise an equation of motion, as the path-probability method [32] or a lattice version of density-functional theory [33]. This is in progress.

ACKNOWLEDGMENTS

We would like to thank W. Dieterich, V. Fleury, T. Gobron, and J. C. Nedelec for many valuable discussions. One of us (M.P.) was supported by a grant from the Ministère de l'Enseignement Supérieur et de la Recherche (MESR). Laboratoire de Physique de la Matière Condensée is Unité de Recherche Associée (URA) 1254 to the Centre National de la Recherche Scientifique (CNRS).

[1] J. W. Cahn and J. E. Hilliard, J. Chem. Phys. **28**, 258 (1958).
[2] J. S. Langer, Rev. Mod. Phys. **52**, 1 (1980).
[3] D. A. Kessler, J. Koplik, and H. Levine, Adv. Phys. **37**, 255 (1988).
[4] Y. Pomeau and M. Ben Amar, in *Solids far from Equilibrium*, edited by C. Godrèche (Cambridge University Press, Cambridge, 1992).
[5] E. Brener and V. Melnikov, Adv. Phys. **40**, 53 (1991); E. Brener, H. Müller-Krumbhaar, and D. Temkin, Europhys. Lett. **17**, 535 (1992); M. Ben Amar and E. Brener, Phys. Rev. Lett. **71**, 589 (1993); E. Brener, *ibid*. **71**, 3653 (1993).
[6] E. Ben-Jacob, P. Garik, T. Mueller, and D. Grier, Phys. Rev. A **38**, 1370 (1988).
[7] H. Biloni and B. Chalmers, Trans. Metall. Soc. AIME **233**, 373 (1965).
[8] J. C. Baker and J. W. Cahn, Acta Metall. **17**, 575 (1969).
[9] M. J. Aziz, J. Appl. Phys. **53**, 1158 (1982); M. J. Aziz and T. Kaplan, Acta Metall. **36**, 2335 (1988); M. J. Aziz and W. J. Boettinger, *ibid*. **42**, 527 (1994); P. M. Smith and M. J. Aziz, *ibid*. **42**, 3515 (1994).
[10] B. Caroli, C. Caroli, and B. Roulet, Acta Metall. **39**, 1867 (1986).
[11] A. A. Wheeler, W. J. Boettinger, and G. B. McFadden, Phys. Rev. E **47**, 1893 (1993).
[12] See, for example, L. I. Rubinstein, *The Stefan Problem* (American Mathematical Society, Providence, 1977).
[13] J. S. Langer and R. F. Sekerka, Acta Metall. **23**, 1225 (1975).
[14] J. S. Langer, in *Directions in Condensed Matter Physics*, edited by G. Grinstein and G. Mazenko (World Scientific, Singapore, 1986).
[15] J. B. Collins and H. Levine, Phys. Rev. B **31**, 6119 (1985).
[16] G. Caginalp and P. Fife, Phys. Rev. B **33**, 7792 (1986).
[17] R. Kupfermann, O. Shochet, E. Ben-Jacob, and Z. Schuss, Phys. Rev. B **46**, 16 045 (1992).
[18] A. J. Bray, Adv. Phys. **43**, 357 (1994).
[19] F. Ducastelle, Prog. Theor. Phys. Suppl. **115**, 273 (1994).
[20] J.-F. Gouyet, Europhys. Lett. **21**, 335 (1993); Phys. Rev. E **51**, 1695 (1995).
[21] M. Plapp and J.-F. Gouyet, Phys. Rev. E **55**, 45 (1997).
[22] R. Pandit and M. Wortis, Phys. Rev. B **25**, 3226 (1982).
[23] T. Sakamoto, N. J. Kawai, T. Nakagawa, K. Ohta, and T. Kojima, Appl. Phys. Lett. **47**, 617 (1985).
[24] H. C. Kang and J. W. Evans, Surf. Sci. **271**, 321 (1992).
[25] R. Baiod, Z. Cheng, and R. Savit, Phys. Rev. B **34**, 7764 (1986).
[26] R. Savit and R. K. P. Zia, J. Phys. A **20**, L987 (1987); Z. Cheng, L. Jacobs, D. Kessler, and R. Savit, *ibid*. **20**, L1095 (1987).
[27] A. Williams, R. Moss, and P. Harrowell, J. Chem. Phys. **99**, 3998 (1993).
[28] K. Kawasaki, Phys. Rev. **145**, 224 (1966).
[29] J. W. Cahn, Trans. Metall. Soc. AIME **242**, 166 (1968).
[30] P. C. Hohenberg and B. I. Halperin, Rev. Mod. Phys. **49**, 435 (1977).
[31] T. Gobron, J. Stat. Phys. **69**, 995 (1992).
[32] H. Sato and R. Kikuchi, J. Chem. Phys. **55**, 677 (1971).
[33] M. Nieswand, A. Majhofer, and W. Dieterich, Phys. Rev. E **48**, 2521 (1993); D. Reinel, W. Dieterich, and A. Majhofer, *ibid*. **50**, 4744 (1994); D. Reinel and W. Dieterich, J. Chem. Phys. **104**, 5234 (1996).